Visualization of Bacterial Colonization and Cellular Layers in a Gut-on-a-Chip System Using Optical Coherence Tomography

Yuan, Lu; de Haan, Pim; Peterson, Brandon W.; de Jong, Ed D.; Verpoorte, Elisabeth; van der Mei, Henny C.; Busscher, Henk J.

Published in:
Microscopy and Microanalysis

DOI:
10.1017/S143192762002454X

Publication date:
2020

Microscopy and Microanalysis (2020), **26**, 1211–1219
doi:10.1017/S143192762002454X

Microscopy AND Microanalysis

Original Article

Visualization of Bacterial Colonization and Cellular Layers in a Gut-on-a-Chip System Using Optical Coherence Tomography

Lu Yuan[1], Pim de Haan[2,3], Brandon W. Peterson[1], Ed D. de Jong[1], Elisabeth Verpoorte[2], Henny C. van der Mei[1]* and Henk J. Busscher[1]

[1]Department of Biomedical Engineering, University of Groningen, University Medical Center Groningen, 9713 AV Groningen, The Netherlands; [2]University of Groningen, Groningen Research Institute of Pharmacy, Pharmaceutical Analysis, 9713 AV Groningen, The Netherlands and [3]TI-COAST, 1098 XH Amsterdam, The Netherlands

Abstract

Imaging of cellular layers in a gut-on-a-chip system has been confined to two-dimensional (2D)-imaging through conventional light microscopy and confocal laser scanning microscopy (CLSM) yielding three-dimensional- and 2D-cross-sectional reconstructions. However, CLSM requires staining and is unsuitable for longitudinal visualization. Here, we compare merits of optical coherence tomography (OCT) with those of CLSM and light microscopy for visualization of intestinal epithelial layers during protection by a probiotic *Bifidobacterium breve* strain and a simultaneous pathogen challenge by an *Escherichia coli* strain. OCT cross-sectional images yielded film thicknesses that coincided with end-point thicknesses derived from cross-sectional CLSM images. Light microscopy on histological sections of epithelial layers at the end-point yielded smaller layer thicknesses than OCT and CLSM. Protective effects of *B. breve* adhering to an epithelial layer against an *E. coli* challenge included the preservation of layer thickness and membrane surface coverage by epithelial cells. OCT does not require staining or sectioning, making OCT suitable for longitudinal visualization of biological films, but as a drawback, OCT does not allow an epithelial layer to be distinguished from bacterial biofilms adhering to it. Thus, OCT is ideal to longitudinally evaluate epithelial layers under probiotic protection and pathogen challenges, but proper image interpretation requires the application of a second method at the end-point to distinguish bacterial and epithelial films.

Key words: CLSM, microfluidic device, OCT, organ-on-a-chip, probiotics

(Received 5 August 2020; revised 8 September 2020; accepted 23 September 2020)

Introduction

The human intestines form a complex ecosystem (Tropini et al., 2017) containing a well-balanced microbial composition (Mitsuoka, 1990; O'Callaghan & Van Sinderen, 2016). When its balanced composition is challenged by opportunistic pathogens such as *Escherichia coli*, disease results (Miskinyte et al., 2013; Proença et al., 2017). Lactobacilli and bifidobacteria form part of the healthy intestinal microflora (Guarner & Malagelada, 2003), protecting the host against opportunistic pathogens (Candela et al., 2008; Fukuda et al., 2011). Probiotic bacteria such as lactobacilli and bifidobacteria are applied more and more to complement the commensal microflora and promote a healthy intestinal microflora (Kleerebezem & Vaughan, 2009). Probiotic bacteria operate through a variety of mechanisms, including competitive inhibition of pathogen adhesion, pathogen displacement, production of bacteriocins and biosurfactants, and modulation of epithelial barrier function (Ohland & MacNaughton, 2010; Reid et al., 2011). Probiotic effects on intestinal epithelial layers have been mostly studied for lactobacilli in well-plates or transwell systems (Miyoshi et al., 2006; Borthakur et al., 2008; Tuo et al., 2013; Gao et al., 2017), but the growth of intestinal epithelial layers in well-plates or transwell systems generally does not yield a villi structure that is characteristic of intestinal epithelial layers in the gut, possibly due to the absence of fluid flow (Kim et al., 2012). Also, the absence of flow makes it difficult to continuously feed the epithelial cell layer and perform long-term studies (Kim et al., 2012). The absence of flow may compromise cellular layers within 1 day (Kim et al., 2012, 2016). Gut-on-a-chip systems in a microfluidic device possess an upper and lower channel, separated by a membrane on which intestinal epithelial cells are grown. Channels can be continuously perfused with growth media facilitating long-term studies. As a result, intestinal epithelial layers grown in a gut-on-a-chip model usually show clear villi (Kim et al., 2012).

Visualization of the complicated three-dimensional structure constituting a cellular layer, particularly with an adhering bacterial biofilm, either probiotic and/or pathogenic, is difficult (Polat et al., 2019). Imaging of cellular layers in lab-on-a-chip systems is usually through planar, two-dimensional conventional light microscopy, impeding analyses of the thickness of the cellular layers and sometimes involving destructive sectioning for histological analyses. Fluorescence microscopy, including confocal laser scanning microscopy (CLSM), requires staining and therewith is destructive, impeding longitudinal evaluation over time.

*Author for correspondence: Henny C. van der Mei, E-mail: h.c.van.der.mei@umcg.nl

Cite this article: Yuan L, de Haan P, Peterson BW, de Jong ED, Verpoorte E, van der Mei HC, Busscher HJ (2020) Visualization of Bacterial Colonization and Cellular Layers in a Gut-on-a-Chip System Using Optical Coherence Tomography. *Microsc Microanal* **26**, 1211–1219. doi:10.1017/S143192762002454X

Moreover, conventional microscopic methods are often biased by observer preferences for publishing "nice" images, covering a typical field-of-view area limited to around 300 μm × 300 μm (Huh et al., 2010; Kim et al., 2012, 2016; Kim & Ingber, 2013; Jalili-Firoozinezhad et al., 2018) or reconstructed cross-sectional images covering field-of-view lengths of around 300 μm (Kim et al., 2012, 2016; Jalili-Firoozinezhad et al., 2018). Also, due to limited stain penetration and light scattering, fluorescence microscopy has a limited depth of information (Graf & Boppart, 2010). Optical coherence tomography (OCT) is a rapid, real-time, *in situ* and nondestructive, low-resolution imaging method, not requiring any staining or sectioning. Its nondestructive nature makes OCT an ideal method for longitudinal visualization of biological films, while its low-resolution is compensated by a relatively large field-of-view area up to 100 mm^2 (Tang et al., 2007). OCT relies on light scattering to measure the scattered signal intensities of a substratum surface, including cellular layers or bacterial biofilms growing on these surfaces. Accordingly, objects exhibiting higher light scattering will yield higher signal intensities, than objects with lower scattering, yielding a signal intensity distribution from which OCT images can be reconstructed based on an artificial greyscale (Dreszer et al., 2014; Hou et al., 2019). In order to measure cellular layer or biofilm thicknesses from an OCT image, the whiteness of a biological film, reflecting high signal intensities, has to be distinguished from the relatively low signal intensity, black background of its aqueous environment. This can be done by proper thresholding (Otsu, 1979) to define the exact position of the biological film surface. Black pixels left inside a biofilm have been ascribed to water-filled pores (Hou et al., 2019). Accordingly, OCT is widely used to measure biofilm thickness (Xi et al., 2006; Janjaroen et al., 2013; Dreszer et al., 2014; Fortunato et al., 2017; Fortunato & Leiknes, 2017), but to the best of our knowledge has not yet found its way for the analysis of cellular layer thicknesses in microfluidic devices, including gut-on-a-chip systems.

The aim of this paper is to evaluate the merits of using OCT as a new imaging method of cellular layers in lab-on-a-chip systems under the complex condition of simultaneous probiotic protection by *Bifidobacterium breve* and a pathogenic *E. coli* challenge. Thicknesses of the resulting biological films will be compared with those of conventional light microscopy, including tiling-mode CLSM.

Materials and Methods

Design and Fabrication of the Microfluidic Device

A gut-on-a-chip microfluidic device (Fig. 1a) was designed as previously described (Huh et al., 2013) with some minor modifications. Polydimethylsiloxane (PDMS; Sylgard 184, Dow Corning, Midland, MI, USA) was mixed with Sylgard® silicone elastomer curing agent (Dow Corning, Midland, MI, USA) at a ratio of 10:1 (w/w). The PDMS mixture was poured onto a microfabricated mold that had been formed by photolithographically patterning of a 150 μm thick layer of SU-8 2100 (Kayaku Advanced Materials, Westborough, MA, USA) onto a flat glass wafer to yield features that allow the replication of in-house designed upper and lower channels (Duffy et al., 1998; De Haan et al., 2019). These channels had a width of 1 mm, a length of 1 cm, and a height of 150 μm. The PDMS was degassed in a vacuum chamber for 30 min and allowed to cure on a hot plate at 70°C for 2 h, after which it was peeled off the master mold with a scalpel and tweezer. Holes of 1.5 mm were punched at the end of the channels with a biopsy puncher. The upper and lower channels were separated by a 30 μm thick collagen-coated polytetrafluoroethylene (PTFE) membrane (Millicell, Merck, Darmstadt, Germany) with a pore size of 0.4 μm. After oxygen plasma treatment (310–320 mTorr, 20 s, Harrick Plasma PDC-0002, Ithaca, NY, USA) of both PDMS parts of the device, the membrane was placed on the lower PDMS channel and the upper PDMS channel was aligned with the lower channel using a dissecting microscope to assemble the device. The PDMS parts of the microfluidic device were pressed to each other and cured at 70°C for 30 min to bind the PDMS parts together. Pieces of PTFE tubing (inner diameter 0.8 mm, outer diameter 1.6 mm, VWR, The Netherlands) were connected to 5 mL syringes (inner diameter 13 mm, Terumo Corporation, Japan) using a needle (21 G Fine-Ject, VWR, The Netherlands) and connected to the medium inlets of the upper and lower channels. PTFE tubing connected the device outlets with a waste-collecting vessel. Media were

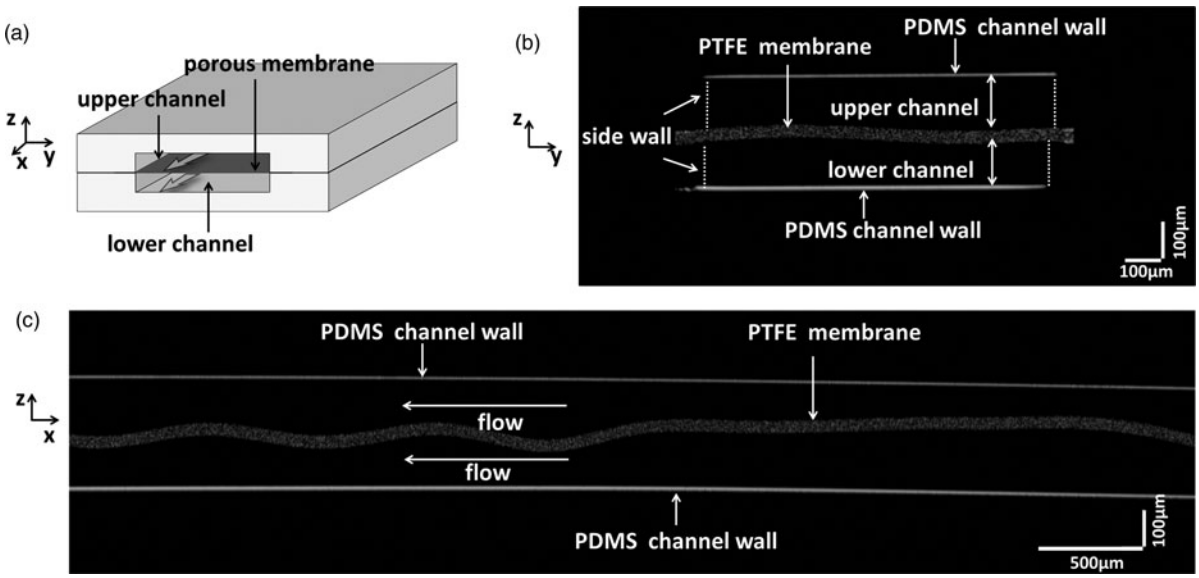

Fig. 1. (**a**) Schematic drawing of a microfluidic device, showing the upper and lower channel separated by a porous membrane. (**b**) OCT cross-sectional image of the porous PTFE membrane taken along the width (*Y*-direction) of the channel, separating the upper and lower channel in a microfluidic device. (**c**) Same as panel (**b**), now along the length (*X*-direction) of the channel.

pumped with a multiple-channel pump (flow rate 30 μL/h, model NE1800, New Era Pump System Inc., Farmingdale, NY, USA) through the microfluidic device. Before starting an experiment, microfluidic devices were sterilized by immersion in 70% ethanol for 30 min and washed three times with sterile phosphate-buffered saline (PBS; 8.1 mM Na_2HPO_4, 137 mM NaCl, 1.5 mM KH_2PO_4, 2.7 mM KCl, pH 7.2).

Epithelial Cells and Harvesting

Human intestinal epithelial cells, Caco-2 BBe1 (ATCC CRL-2102), were cultured in Dulbecco's Modified Eagle Medium containing 4.5 g/L glucose (DMEM-HG; Gibco, Thermo Fisher Scientific, Waltham, MA, USA) supplemented with 10% (v/v) fetal bovine serum (FBS; Gibco) in 5% CO_2 at 37°C. Epithelial cells were passaged upon reaching 80% confluency, washed twice in sterile PBS, and detached with 3 mL trypsin/EDTA (2.5 g/L, Gibco, USA) from a T-75 flask at 37°C for 5 min. Subsequently, 6 mL DMEM-HG with 10% FBS was added, and the epithelial cell suspension was centrifuged at 800 *g* for 5 min. Finally, cells were suspended in DMEM-HG supplemented with 10% FBS at a density of 10^7 mL^{-1}, as determined using an automated cell counter (Merck Millipore, Burlington, MA, USA).

Bacterial Strains and Harvesting

B. breve ATCC 15700 was obtained from American Type Culture Collection (ATCC; Manassas, VA, USA) and applied as a probiotic strain. *E. coli* Hu734 is a human clinical isolate and was used as a pathogenic strain. *B. breve* was streaked from frozen stock on a reinforced clostridial medium agar plate (RCM; Becton, Dickinson and Company, Franklin Lakes, NJ, USA) and cultured under anaerobic conditions (85% N_2, 5% CO_2, 10% H_2) at 37°C for 48 h. *E. coli* was streaked on a blood agar plate and cultured aerobically at 37°C for 24 h. One colony of *B. breve* or *E. coli* was transferred in 10 mL RCM and Luria-Bertani broth (LB; Sigma-Aldrich, St. Louis, MO, USA), respectively. After 24 h, strains were transferred (1:20) into fresh growth medium and grown for another 18 h. Bacteria were harvested by centrifugation at 6,500 *g* at 10°C for 5 min, washed twice with sterile PBS, and re-suspended in PBS to the concentrations required for further experiments, as determined using a Bürker-Türk counting chamber.

Growth of Epithelial Cell Layers and Bacterial Biofilms

After assembly of the microfluidic device and rinsing it with PBS, the upper channel was perfused with extracellular matrix (ECM) solution containing 300 μg/mL ECM proteins (Matrigel matrix, Corning Inc., Corning, NY, USA) and 50 μg/mL type I collagen (Advanced BioMatrix, San Diego, CA, USA) in DMEM-HG in 5% CO_2 at 37°C to coat the membrane and channel walls. After 16 h, the channel was washed with 2 mL PBS, and epithelial cells were seeded from suspension (1×10^7 mL^{-1}) in the upper channel on the ECM-coated membrane to a density of 1.5×10^5 cm^{-2} by sedimentation. After 2 h sedimentation, both channels were perfused with DMEM-HG supplemented with 20% (v/v) FBS at the volumetric flow rate of 30 μL/h for 7 days.

Next *E. coli* (10^5 mL^{-1}) or *B. breve* (10^7 mL^{-1}) were allowed to sediment from suspension in the upper channel to the epithelial cell layer. After 2 h sedimentation, the upper channel was perfused with the modified culture medium (70% DMEM-HG with 20% FBS cell culture medium and 30% RCM), suitable to grow *B. breve* and intestinal epithelial cells. The lower channel was perfused with DMEM-HG with 20% FBS to optimally facilitate epithelial cell growth. A similar procedure was used to evaluate the protection of intestinal epithelial cells offered by *B. breve* against a pathogenic *E. coli* challenge. To this end, *B. breve* (10^7 mL^{-1}) were first allowed to sediment in the upper channel and grow a protective film on an epithelial cell layer on the membrane for 48 h that was subsequently challenged with *E. coli* (10^5 mL^{-1}) for another 48 h.

Visualization of the Cellular Layers in the Absence and Presence of a Bacterial Biofilm

Optical Coherence Tomography

In situ membranes with or without intestinal epithelial cells and bacterial biofilms were longitudinally imaged without staining or other preparation using an OCT Ganymede-II Spectral Domain (Thorlabs Inc., Newton, NJ, USA) with 930 nm center wavelength laser. The refractive index of the biological films was set at 1.33, equal to the one of water. OCT cross-sectional images along the *Z*-direction with a field-of-view area of 4×1 mm^2 (5,000 px × 373 px) were taken at a Z resolution of 4.4 μm using a 5× telecentric scan lens. Images were taken at different time points during growth after which the microfluidic devices were placed back into the incubator. Ten images per time point were taken randomly divided over each biological film on a membrane. OCT signal intensities were processed with the ThorImage OCT 4.1 software, and thicknesses of the membranes with and without cellular layers and/or bacterial biofilms were derived from cross sections using Otsu thresholding (Otsu, 1979).

Confocal Laser Scanning Microscopy

At the end of an experiment, the channels were washed twice with PBS and cellular layers with or without bacterial biofilms were fixed with 3.7% paraformaldehyde for 30 min followed by permeabilization with 0.5% Triton X-100 for 5 min. Next, staining was done with Phalloidin (diluted 50× in PBS with 1% bovine serum albumin, Sigma-Aldrich, St. Louis, MO, USA) and 4′,6-diamidino-2-phenylindole dihydrochloride (DAPI; diluted 50× in PBS with 1% bovine serum albumin, Sigma-Aldrich, St. Louis, MO, USA) for 1 h to visualize F-actins (495 nm excitation/520 nm emission) of the epithelial cells and DNA (364 nm excitation/454 nm emission), respectively. Epithelial cells and bacteria were imaged using a CLSM (Leica SP8, Germany). Images were taken over an *X*–*Y* field-of-view area of $1{,}164 \times 1{,}164$ μm^2 (512 px × 512 px) at a Z-stack distance of 5 μm. The use of Fiji software allowed to overlap 12 images ("tiling-mode") facilitating the reconstruction of an image of the entire membrane area. The surface coverage of the membrane by the epithelial cells and layer thickness could also be derived using Fiji software.

Phase-Contrast Microscopy

The intestinal epithelial cell layers on the membrane were observed daily during growth in the microfluidic device using phase-contrast microscopy (Leica DMIL, Wetzlar, Germany). Images were taken at a field-of-view area of 0.92 mm^2 (microscope magnification 100×).

Histological Analyses

For histological analyses, the epithelial cell layers and bacterial biofilms in the microfluidic devices were washed twice with PBS and fixed with 3.7% paraformaldehyde for 30 min. After fixation, the microfluidic device was opened with a scalpel and the membrane with the epithelial cell layers and bacterial biofilms was carefully removed, keeping the epithelial cell layers intact. The membrane

with biological films was dehydrated in a series of ethanol–water solutions with increasing ethanol % (35, 50, 60, 70, 80, 85, 90, 95, 100, and 100% again) for 15 min each, prior to embedding. The dehydrated samples were then embedded in glycol methacrylate (Technovit® 7100, VWR, Amsterdam, The Netherlands). To this end, samples were first immersed in an infiltrating solution (100% ethanol/Technovit® 7100 with hardener 1 at volume ratios of 1:2) for 16 h. Then, samples were transferred for hardening to an inclusion solution (Technovit® 7100 with hardener 1 and hardener 2) for 4 h at room temperature, and 5 μm sections were cut with a Leica RM2165 microtome. Samples were stained with toluidine blue (Sigma-Aldrich) to observe cells and bacteria. Briefly, the samples were stained with toluidine blue for 1 min, washed with water for 1 min, and images were taken with a light microscope at a field-of-view area of 0.24 mm^2 (microscope magnification 200×) (Sridharan & Shankar, 2012).

Statistical Analysis

All results were expressed as means ± standard errors of mean (SEM). A one-way analysis of variance with Tukey multiple comparisons was performed with GraphPad Prism 7 to identify significant differences between groups. Differences were considered statistically significant when $p < 0.05$.

Results

Membrane Visualization in a Microfluidic Device Using OCT

The thickness of the PTFE membrane in the microfluidic devices used (Fig. 1a) was found to be 35 ± 2 μm, as measured from OCT cross-sectional images (Figs. 1b, 1c).

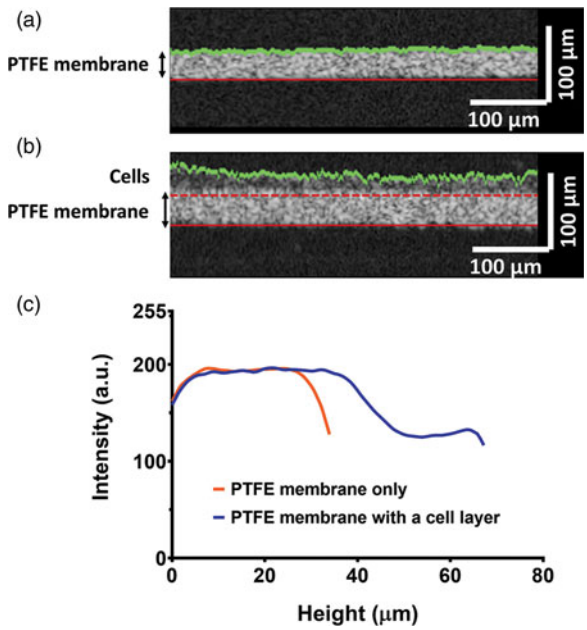

Fig. 2. (**a**) OCT cross-sectional image of a PTFE membrane in a microfluidic device, in the absence of a biological layer. (**b**) OCT cross-sectional image of an epithelial cell layer, grown on the PTFE membrane. The green line represents the top of the cellular layer, while the dotted and solid red lines represent the top and the bottom of the membrane separating both channels, respectively. All images are taken in the length (*X*-direction) of the channel. (**c**) OCT signal intensity as a function of layer thickness, including the PTFE membrane and cellular layer.

Cellular Layer Thickness and Villi Visualization Using OCT

OCT cross-sectional images of a microfluidic device in the absence and presence of an epithelial cell layer grown for 3 days on the membrane are shown in Figures 2a and 2b, respectively. The epithelial cells can be easily discriminated from the membrane with OCT due to the difference in signal intensities (Fig. 2c).

Longitudinal monitoring of the thickness of a cellular layer in the same microfluidic device (Fig. 3) using OCT demonstrated that cells achieved a 100% confluency after 3 days of growth as visualized using phase-contrast microscopy (Fig. S1). Confluency was maintained for up to at least 10 days in the same microfluidic device, as confirmed by phase-contrast

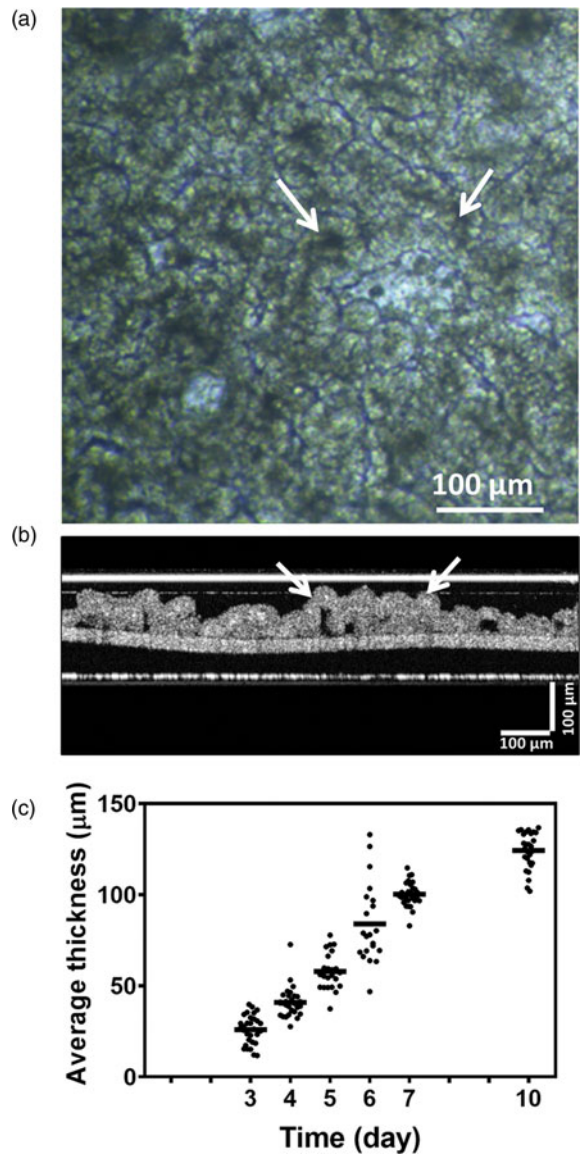

Fig. 3. (**a**) Phase-contrast microscope image of an intestinal epithelial Caco-2 BBe1 cell layer (top-view), grown for 7 days on a PTFE membrane in a microfluidic device (see Fig. 1b). White arrows indicate villi. (**b**) OCT cross-sectional image of the above Caco-2 BBe1 cell layer. Image is taken in the length (*X*-direction) of the channel. White arrows indicate villi. (**c**) Epithelial cell layer thickness, including villi, as a function of growth time averaged over an entire field-of-view area (4 × 1 mm). Ten images taken at random locations over one cellular layer. Experiments were done with three microfluidic devices simultaneously, yielding a total of 30 data points per time point.

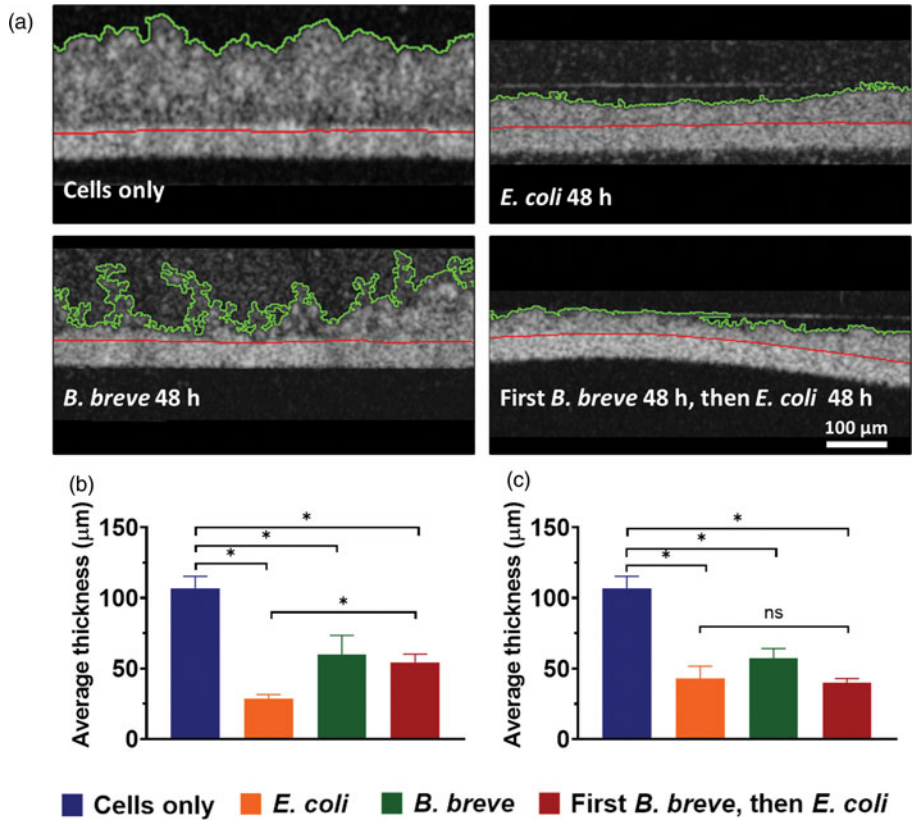

Fig. 4. (**a**) OCT cross-sectional images of intestinal epithelial Caco-2 BBe1 cells grown for 7 days on a PTFE membrane in a microfluidic device (cells only). Seven-day-old epithelial cell layers were also co-cultured with *E. coli* or *B. breve* separately for 48 h or subjected to an *E. coli* challenge under *B. breve* protection (first *B. breve* alone for 48 h after which *E. coli* were added for another 48 h). The red lines indicate the top of the membrane, while the green lines indicate the outer surface of the epithelial cell layer, including a bacterial biofilm. Images are taken in the length (*X*-direction) of the channel. (**b**) Average biological layer thicknesses of epithelial cell layers cultured for 7 days, co-cultured with *E. coli* or *B. breve* separately for 24 h, and co-cultured with *B. breve* for 48 h and then subjected to an *E. coli* challenge for another 24 h. (**c**) Same as panel (**b**), now for cellular layers co-cultured with *E. coli* or *B. breve* separately for 48 h, and co-cultured with *B. breve* for 48 h and then subjected to an *E. coli* challenge for another 48 h. Error bars represent SEM over three experiments with separately grown cells and bacteria. Asterisks indicate statistically significant differences $p < 0.05$, while *ns* indicates the absence of statistically significant difference.

microscopy (Fig. 3a) and OCT cross-sectional images of the cellular layer (Fig. 3b). Villi could be observed in phase-contrast (Fig. 3a) as well as in OCT cross-sectional (Fig. 3b) images. Layer thickness, excluding the membrane thickness but including cells and villi formed, were measured in the same microfluidic device over the course of an experiment (Fig. 3c), showing a linear increase till day 7 (100 μm) and reaching a stationary thickness after 10 days (124 μm). The thickness reached after 10 days is close to the depth of the channel (150 μm) of the microfluidic device, possibly indicating that growth was restricted by the channel walls as can be seen in OCT cross-sectional images (Fig. 3b). To avoid channel wall-restricted growth and associated membrane deformation (see also Fig. 3b), all epithelial cell layers were cultured for 7 days in further experiments.

Intestinal Epithelial Cell Layers with Adhering Bacteria Visualized Using OCT

After 7 days of epithelial cell growth, an epithelial cell layer was first challenged with *E. coli* (10^5 mL^{-1}) or *B. breve* (10^7 mL^{-1}) and co-cultured for 48 h (Fig. 4a). Unfortunately, the OCT images did not allow cellular layers to be distinguished from bacterial biofilms; hence, we could only observe what we call here "a biological film". *E. coli* strongly reduced the biological film thickness on the top of the membrane as compared with the cellular layer thickness observed in the absence of adhering bacteria. Adhesion of *B. breve* in the absence of challenging *E. coli* yielded a thin biological film with an irregularly shaped surface. In order to study the protection of *B. breve* against a simultaneous *E. coli* challenge, epithelial cells were first co-cultured with *B. breve* (10^7 mL^{-1}) for 48 h and then *E. coli* (10^5 mL^{-1}) were introduced and co-cultured for another 24 or 48 h. This too yielded a reduced biological film thickness as compared with an epithelial layer in the absence of adhering bacteria. Quantitative evaluation of the thicknesses of the biological films, i.e., cells and bacteria, was done after Otsu thresholding (Otsu, 1979) to distinguish the total biological layer thickness from the background. However, it was not possible to distinguish, which fraction of the thickness was due to the cellular layer and which was due to the bacterial biofilm (Figs. 4b, 4c). The total thickness of the biological film was significantly decreased upon an *E. coli* challenge as well as during *B. breve* adhesion for 24 h (Fig. 4b) or 48 h (Fig. 4c). A 24 h *E. coli* challenge under *B. breve* protection yielded a significantly smaller decrease in biological film thickness than observed in the absence of *B. breve* protection (Fig. 4b). Forty eight h *B. breve* protection followed by a 48 h *E. coli* challenge, however, did not point to any protection of the epithelial cell layer.

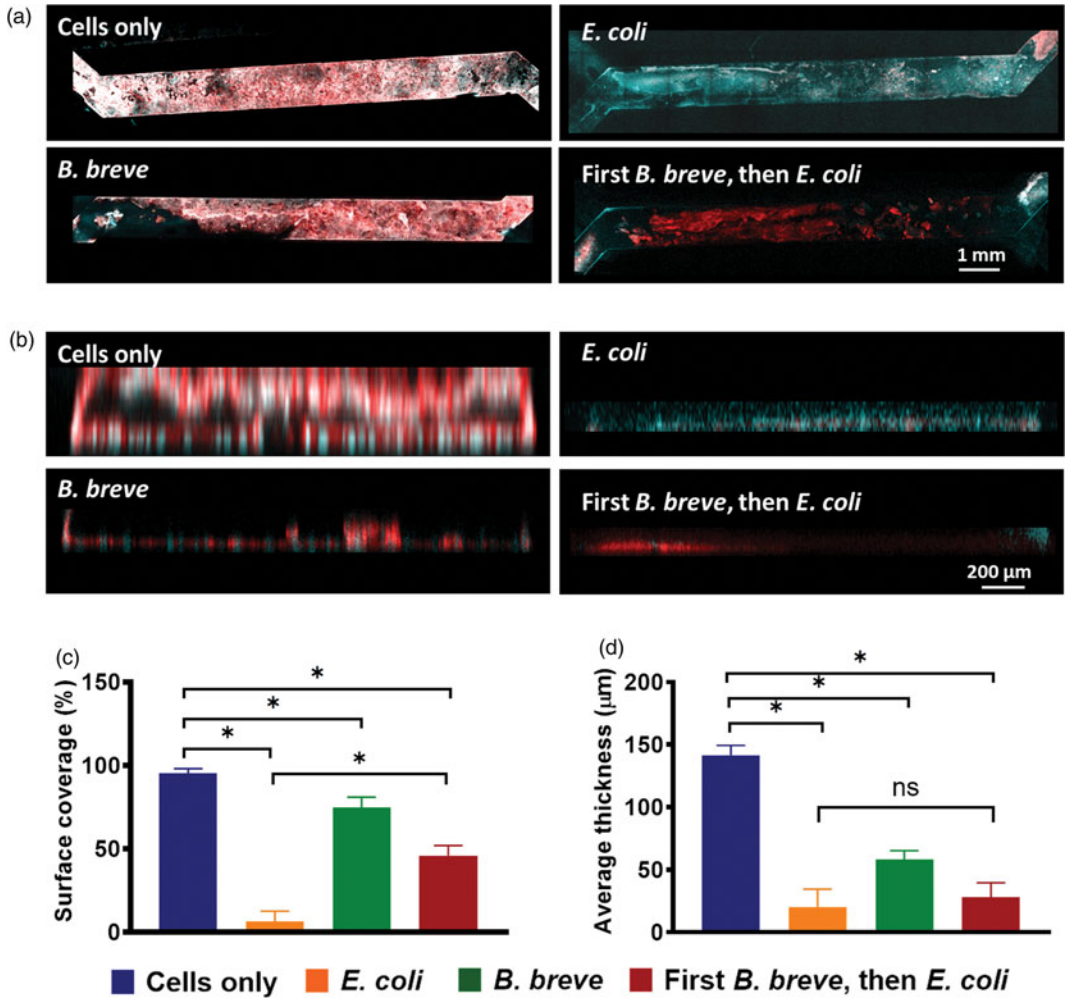

Fig. 5. (**a**) Tiling-mode CLSM overlayer images of intestinal epithelial Caco-2 BBe1 cells grown for 7 days on a PTFE membrane in a microfluidic device (cells only). Seven-day-old epithelial layers were also co-cultured with *E. coli* or *B. breve* separately for 48 h or subsequently subjected to an *E. coli* challenge (first *B. breve* alone for 48 h after which *E. coli* were added for another 48 h). (**b**) Same as panel (**a**), now for CLSM cross-sectional images. Images are taken in the width direction of the channel. Cells and bacteria were stained with Phalloidin (red-fluorescent, cytoskeleton) and DAPI (blue-fluorescent, DNA). (**c**) Surface coverage of the PTFE membrane in the microfluidic device by intestinal epithelial cells in the absence and presence of bacterial biofilms, taken from CLSM overlayer images, as presented in panel (**a**). (**d**) Average thickness of biological films, including intestinal epithelial cell layers and bacterial biofilms, taken from tiling-mode CLSM cross-sectional images, as presented in panel (**b**). Error bars represent SEM over three experiments with separately grown cells and bacteria. Asterisks indicate statistically significant differences, $p < 0.05$, while *ns* indicates the absence of statistically significant difference.

Intestinal Epithelial Cell Layers with Adhering Bacteria Visualized Using Tiling-Mode CLSM

The epithelial cell layers grown in the absence and presence of adhering bacteria in the microfluidic device were stained with red-fluorescent Phalloidin and blue-fluorescent DAPI and visualized using CLSM (Figs. 5a, 5b). The epithelial cell layer almost completely covered the membrane surface as concluded from the red-fluorescence. Membrane surface coverage by the epithelial cell layer was nearly fully destroyed upon an *E. coli* challenge (Fig. 5a). After a 48 h *E. coli* challenge, only blue-fluorescence remained, attributed to the presence of the *E. coli* biofilm. In contrast, when co-cultured for 48 h with probiotic *B. breve*, membrane surface coverage by epithelial cells remained high. Moreover, adhesion of *B. breve* to epithelial cell layers for 48 h protected the cellular layer against a 48 h *E. coli* challenge and membrane surface coverage was better maintained than in the absence of adhering *B. breve*.

Analyses of the cell surface coverage of the membrane in CLSM overlayer images (Fig. 5c) aided the interpretation of biological film thicknesses using OCT (Fig. 4) in the sense that they clearly indicated in which case the biological film thicknesses should be attributed to epithelial cells or a combination of epithelial cells with an adhering bacterial biofilm. Interestingly, decreases in surface coverage were concurrent with decreases in the total thickness of the stained layers in cross-sectional CLSM images (compare Figs. 5c, 5d) and in line with the decreases in biological film thicknesses taken from OCT cross-sectional images (Fig. 4). The concurrence of decreases in surface coverage by Phalloidin/DAPI stained cellular layers with decreases in biological layer thickness suggests that the thickness of bacterial biofilms may be negligible as compared with cellular layer thicknesses.

Light Microscopy on Histological Sections of Intestinal Epithelial Cell Layers with Adhering Bacteria

Histological sections of intestinal epithelial cell layers in the absence and presence of adhering bacteria were stained with

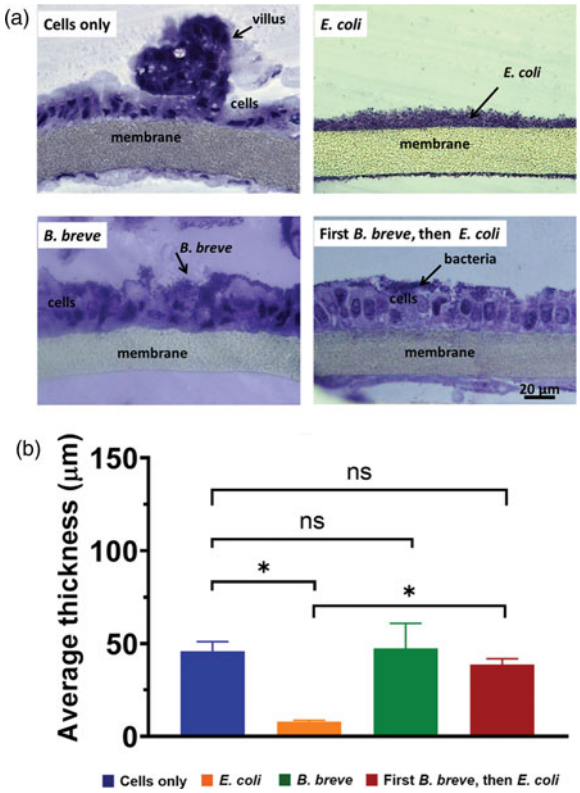

Fig. 6. (**a**) Light microscopic images of histological cross sections of intestinal epithelial Caco-2 BBe1 cell layers grown for 7 days on a PTFE membrane in a microfluidic device (cells only). Seven-day-old epithelial cell layers were also co-cultured with *E. coli* or *B. breve* separately for 48 h, or subjected to an *E. coli* challenge under *B. breve* protection (first *B. breve* alone for 48 h after which *E. coli* were added for another 48 h). (**b**) Average thickness of epithelial cells layers cultured for 7 days, co-cultured with *E. coli* or *B. breve* separately for 48 h, and co-cultured with *B. breve* for 48 h and then subjected to an *E. coli* challenge for another 48 h. Error bars represent SEM over three experiments with separately grown cells and bacteria. Asterisks indicate statistically significant differences $p < 0.05$, while *ns* indicates the absence of statistically significant difference.

toluidine blue for light microscopical visualization. Epithelial cell layers in the absence of adhering bacteria could be clearly distinguished from the membrane surface on which they were growing, with clearly visible villi (Fig. 6a). Visualization of histological sections furthermore confirmed that an *E. coli* challenge led to the full destruction of the cellular layer and justified the suggestion based on CLSM overlaid images that only a thin *E. coli* layer remained present on the membrane after the challenge. Also, visualization of cellular layers protected by adhering *B. breve* under *E. coli* challenge demonstrated intact cellular layers, and indicate that the bacterial biofilm thickness was negligible compared with the cellular layer thickness (Fig. 6b).

Discussion

This study was carried out with a dual aim in mind. The first aim was to evaluate the merits of OCT imaging of intestinal epithelial cell layers in a gut-on-a-chip system *viz-a-viz* other imaging methods in the complex scenario of probiotic *B. breve* protection of cellular layers during a simultaneous pathogenic *E. coli* challenge. The second aim was to provide insights into beneficial effects of probiotic protection of intestinal epithelial cell layers against a pathogenic challenge in a microfluidic device. Successful growth of an intestinal epithelial layer possessing villi after 7 days of growth followed from phase-contrast microscopy (Fig. 3a), OCT cross-sectional images (Fig. 3b), and light microscopy on histological sections (Fig. 6b). Note that in 3-day-old epithelial layers, no villi could be discerned (Fig. S1).

The application of OCT for visualizing cellular layers in lab-on-a-chip systems has several obvious advantages, most notably its fully nondestructive nature eliminating the need for staining or sectioning. With this, OCT is the only imaging technique suited to longitudinal visualization over time. Visualization of the biological film over the entire membrane area can be done within 5 min using OCT, while CLSM requires 12 images that need to be tiled to create an image over a similar field of view. This requires much more time, roughly 30 min, than needed for OCT imaging of the same field of view, taking only 2 min. This is in addition to the time required for staining of cellular layers and biofilms for CLSM. OCT can visualize the behavior of the membrane and cell growth along the length of the channel (Fig. 3b). Moreover, OCT allowed the observation that cell growth was restricted by the channel height at different locations along the channel wall (Fig. 4a). Channel height-restricted growth can either be missed or appear exaggerated using visualization methods with a smaller field-of-view length such as CLSM (unless used in a tiling-mode). Despite its limited depth of information, tiling-mode CLSM could visualize restricted growth over the entire height of 150 μm (Fig. 5b) of the microfluidic device. Thus, scattering of fluorescent light is not a limiting factor in visualizing epithelial cell layers with a height up to at least 150 μm, consistent with the penetration depth of CLSM reported by Sattler et al. (2013) of around 250 μm. As a drawback, OCT signal intensities do not allow researchers to be able to tell the difference between bacterial and cellular layers. Visualization of sub-cellular structures or single bacteria-cell contact is also not possible (Bousi et al., 2010). Light microscopical visualization of histological sections provided most biological detail, including villi structures, sub-cellular structures, and clearly distinguishable bacterial biofilms and cellular layers (Fig. 6a). Important with respect to understanding the effects of bacterial biofilms adhering to the epithelial cell layers, histological images indicate that the thickness of bacterial biofilms is negligible compared with the epithelial cell layer thickness. This confirms the suggestion based on CLSM overlayer images of Phalloidin/DAPI stained cellular layers to consider the biological film thickness as being predominantly due to cells when surface coverage is high. Thus, biological film thicknesses by OCT can be interpreted within a small margin of error to be representative for the epithelial cell layer thickness.

In Figure 7a, the epithelial cell layer thicknesses as derived for different experimental conditions and measured using OCT are plotted versus thicknesses derived using CLSM or from histological sections. Thicknesses derived using tiling-mode CLSM hover around the line of identity, indicating that both visualization methods yield comparable thicknesses. Also, the SEM of both methods are comparable (Fig. 7b). Histological sections, however, yield significantly smaller thicknesses than OCT and CLSM, possibly due to dehydration during sectioning of the cellular layer. An important drawback of histological sectioning is that decreases in cellular layer thickness due to bacterial presence with respect to layers comprising only cells were not observed (Fig. 6b), except when cellular layers had completely disappeared due to an *E. coli* challenge while unprotected by *B. breve* (Fig. 7b).

These harmful effects of *B. breve* in a microfluidic device are likely due to the fact that epithelial cells were colonized solely

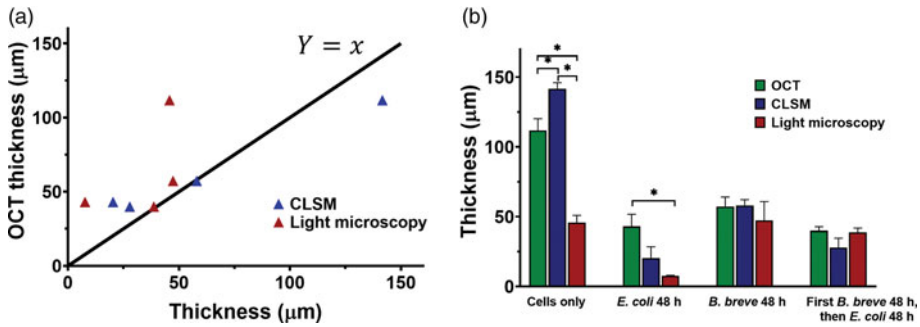

Fig. 7. (**a**) Comparison of average biological film thicknesses including the cellular layers and bacterial biofilms, measured with OCT, CLSM, and light microscopy on histological sections. (**b**) Summary of intestinal epithelial Caco-2 BBe1 cell layers in the absence (cells only) and presence of *E. coli* or *B. breve*, and in the presence of *B. breve* and a simultaneous challenge by *E. coli* (for details, see Figs. 4b, 4c, Figs. 5c, 5d, and Fig. 6b).

by *B. breve* without balancing of their growth by other intestinal bacterial strains. This reflects that overgrowth of epithelial layers by probiotic bacteria can be harmful. This reflects that overdosing daily intake should be avoided, with clinical symptoms such as diarrhea (Rao et al., 2018). In combination with a pathogenic *E. coli* challenge; however, beneficial probiotic effects of *B. breve* protection are clearly shown by the preservation of the epithelial cell layer thickness at the same level as during *B. breve* adhesion in the absence of an *E. coli* challenge (Fig. 7b). Also, *E. coli* were unable to fully destroy an epithelial cell layer under *B. breve* protection.

Conclusion

OCT is the only real-time, fast method to visualize membrane behavior and longitudinally visualize epithelial cell layers in microfluidic devices. Epithelial cell layer thicknesses measured with OCT coincided with end-point thicknesses obtained using CLSM after staining but were larger than obtained from histological sections. As a drawback of OCT, measured thicknesses of biological films with adhering bacteria could not be broken down into bacterial biofilm thickness and cellular layer thickness. Proper interpretation of OCT images of cellular layers with an adhering bacterial biofilm can be done using additional CLSM or histological end-point analyses. In this way, protective effects of *B. breve* adhering to an epithelial cell layer against an *E. coli* challenge could be clearly visualized from the measurement of layer thickness and membrane surface coverage by epithelial cells.

Supplementary material. To view supplementary material for this article, please visit https://doi.org/10.1017/S143192762002454X

Acknowledgments. This work was funded by the University Medical Center Groningen, Groningen, The Netherlands. PdH and EV acknowledge funding from the Dutch Research Council (NWO) in the framework of the Technology Area PTA-COAST3 (GUTTEST, Project #053.21.116) of the Fund New Chemical Innovations.

Conflict of interest. H.J.B. is also director of a consulting company SASA BV. The authors declare no potential conflicts of interest with respect to authorship and/or publication of this article. Opinions and assertions contained herein are those of the authors and are not construed as necessarily representing views of the funding organization or their respective employer(s).

References

Borthakur A, Gill RK, Tyagi S, Koutsouris A, Alrefai WA, Hecht GA, Ramaswamy K & Dudeja PK (2008). The probiotic *Lactobacillus acidophilus* stimulates chloride/hydroxyl exchange activity in human intestinal epithelial cells. *J Nutr* **138**, 1355–1359.

Bousi E, Charalambous I & Pitris C (2010). Optical coherence tomography axial resolution improvement by step-frequency encoding. *Opt Express* **18**, 11877–11890.

Candela M, Perna F, Carnevali P, Vitali B, Ciati R, Gionchetti P, Rizzello F, Campieri M & Brigidi P (2008). Interaction of probiotic *Lactobacillus* and *Bifidobacterium* strains with human intestinal epithelial cells: Adhesion properties, competition against enteropathogens and modulation of IL-8 production. *Int J Food Microbiol* **125**, 286–292.

De Haan P, Ianovska MA, Mathwig K, Van Lieshout GAA, Triantis V, Bouwmeester H & Verpoorte E (2019). Digestion-on-a-chip: A continuous-flow modular microsystem recreating enzymatic digestion in the gastrointestinal tract. *Lab Chip* **19**, 1599–1609.

Dreszer C, Wexler AD, Drusová S, Overdijk T, Zwijnenburg A, Flemming HC, Kruithof JC & Vrouwenvelder JS (2014). In-situ biofilm characterization in membrane systems using optical coherence tomography: Formation, structure, detachment and impact of flux change. *Water Res* **67**, 243–254.

Duffy DC, McDonald JC, Schueller OJA & Whitesides GM (1998). Rapid prototyping of microfluidic systems in poly(dimethylsiloxane). *Anal Chem* **70**, 4974–4984.

Fortunato L & Leiknes T (2017). In-situ biofouling assessment in spacer filled channels using optical coherence tomography (OCT): 3D biofilm thickness mapping. *Bioresour Technol* **229**, 231–235.

Fortunato L, Qamar A, Wang Y, Jeong S & Leiknes T (2017). In-situ assessment of biofilm formation in submerged membrane system using optical coherence tomography and computational fluid dynamics. *J Membr Sci* **521**, 84–94.

Fukuda S, Toh H, Hase K, Oshima K, Nakanishi Y, Yoshimura K, Tobe T, Clarke JM, Topping DL, Suzuki T, Taylor TD, Itoh K, Kikuchi J, Morita H, Hattori M & Ohno H (2011). *Bifidobacteria* can protect from enteropathogenic infection through production of acetate. *Nature* **469**, 543–549.

Gao K, Wang C, Liu L, Dou X, Liu J, Yuan L, Zhang W & Wang H (2017). Immunomodulation and signaling mechanism of *Lactobacillus rhamnosus* GG and its components on porcine intestinal epithelial cells stimulated by lipopolysaccharide. *J Microbiol Immunol Infect* **50**, 700–713.

Graf BW & Boppart SA (2010). Imaging and analysis of three-dimensional cell culture models. *Methods Mol Biol* **591**, 211–227.

Guarner F & Malagelada J-R (2003). Gut flora in health and disease. *Lancet* **361**, 512–519.

Hou J, Wang C, Rozenbaum RT, Gusnaniar N, De Jong ED, Woudstra W, Geertsema-Doornbusch GI, Atema-Smit J, Sjollema J, Ren Y, Busscher HJ & Van der Mei HC (2019). Bacterial density and biofilm structure determined by optical coherence tomography. *Sci Rep* **9**, 9794.

Huh D, Kim HJ, Fraser JP, Shea DE, Khan M, Bahinski A, Hamilton GA & Ingber DE (2013). Microfabrication of human organs-on-chips. *Nat Protoc* **8**, 2135–2157.

Huh D, Matthews BD, Mammoto A, Montoya-Zavala M, Hsin HY & Ingber DE (2010). Reconstituting organ-level lung functions on a chip. *Science* **328**, 1662–1668.

Jalili-Firoozinezhad S, Prantil-Baun R, Jiang A, Potla R, Mammoto T, Weaver JC, Ferrante TC, Kim HJ, Cabral JMS, Levy O & Ingber DE (2018). Modeling radiation injury-induced cell death and countermeasure drug responses in a human gut-on-a-chip article. *Cell Death Dis* **9**, 223.

Janjaroen D, Ling F, Monroy G, Derlon N, Mogenroth E, Boppart SA, Liu WT & Nguyen TH (2013). Roles of ionic strength and biofilm roughness on adhesion kinetics of *Escherichia coli* onto groundwater biofilm grown on PVC surfaces. *Water Res* **47**, 2531–2542.

Kim HJ, Huh D, Hamilton G & Ingber DE (2012). Human gut-on-a-chip inhabited by microbial flora that experiences intestinal peristalsis-like motions and flow. *Lab Chip* **12**, 2165–2174.

Kim HJ & Ingber DE (2013). Gut-on-a-chip microenvironment induces human intestinal cells to undergo villus differentiation. *Integr Biol* **5**, 1130–1140.

Kim HJ, Li H, Collins JJ & Ingber DE (2016). Contributions of microbiome and mechanical deformation to intestinal bacterial overgrowth and inflammation in a human gut-on-a-chip. *Proc Natl Acad Sci* **113**, E7–E15.

Kleerebezem M & Vaughan EE (2009). Probiotic and gut lactobacilli and bifidobacteria: Molecular approaches to study diversity and activity. *Annu Rev Microbiol* **63**, 269–290.

Miskinyte M, Sousa A, Ramiro RS, de Sousa JAM, Kotlinowski J, Caramalho I, Magalhães S, Soares MP & Gordo I (2013). The genetic basis of *Escherichia coli* pathoadaptation to macrophages. *PLoS Pathog* **9**, e1003802.

Mitsuoka T (1990). Bifidobacteria and their role in human health. *J Ind Microbiol* **6**, 263–267.

Miyoshi Y, Okada S, Uchimura T & Satoh E (2006). A mucus adhesion promoting protein, MapA, mediates the adhesion of *Lactobacillus reuteri* to caco-2 human intestinal epithelial cells. *Biosci Biotechnol Biochem* **70**, 1622–1628.

O'Callaghan A & Van Sinderen D (2016). Bifidobacteria and their role as members of the human gut microbiota. *Front Microbiol* **7**, 925.

Ohland CL & MacNaughton WK (2010). Probiotic bacteria and intestinal epithelial barrier function. *Am J Physiol Gastrointest Liver Physiol* **298**, G807–G819.

Otsu N (1979). Threshold selection method from gray-level histograms. *IEEE Trans Syst Man Cybern* **9**, 62–66.

Polat A, Hassan S, Yildirim I, Oliver LE, Mostafaei M, Kumar S, Maharjan S, Bourguet L, Cao X, Ying G, Hesar EM & Zhang YS (2019). A miniaturized optical tomography platform for volumetric imaging of engineered living systems. *Lab Chip* **19**, 550–561.

Proença JT, Barral DC & Gordo I (2017). Commensal-to-pathogen transition: One-single transposon insertion results in two pathoadaptive traits in *Escherichia coli*-macrophage interaction. *Sci Rep* **7**, 4504.

Rao SSC, Rehman A, Yu S & de Andino NM (2018). Brain fogginess, gas and bloating: A link between SIBO, probiotics and metabolic acidosis article. *Clin Transl Gastroenterol* **9**, 162.

Reid G, Younes JA, Van der Mei HC, Gloor GB, Knight R & Busscher HJ (2011). Microbiota restoration: Natural and supplemented recovery of human microbial communities. *Nat Rev Microbiol* **9**, 27–38.

Sattler ECE, Poloczek K, Raphaela K & Welzel J (2013). Confocal laser scanning microscopy and optical coherence tomography for the evaluation of the kinetics and quantification of wound healing after fractional laser therapy. *J Am Acad Dermatol* **69**, 165–173.

Sridharan G & Shankar A (2012). Toluidine blue: A review of its chemistry and clinical utility. *J Oral Maxillofac Pathol* **16**, 251–255.

Tang S, Sun C-H, Krasieva TB, Chen Z & Tromberg BJ (2007). Imaging subcellular scattering contrast by using combined optical coherence and multiphoton microscopy. *Opt Lett* **32**, 503–505.

Tropini C, Earle KA, Huang KC & Sonnenburg JL (2017). The gut microbiome: Connecting spatial organization to function. *Cell Host Microbe* **21**, 433–442.

Tuo Y, Yu H, Ai L, Wu Z, Guo B & Chen W (2013). Aggregation and adhesion properties of 22 Lactobacillus strains. *J Dairy Sci* **96**, 4252–4257.

Xi C, Marks DL, Schlachter S, Luo W & Boppart SA (2006). High-resolution three-dimensional imaging of biofilm development using optical coherence tomography. *J Biomed Opt* **11**, 034001.